Biophysical Journal, Volume *117*

Supplemental Information

Unusual Organization of I-BAR Proteins on Tubular and Vesicular Membranes

Zack Jarin, Feng-Ching Tsai, Aram Davtyan, Alexander J. Pak, Patricia Bassereau, and Gregory A. Voth

Supporting Material for

Unusual Organization of I-BAR Proteins on Tubular and Vesicular Membranes

Z Jarin, F-C Tsai, A Davtyan, A J Pak, P Bassereau, G A Voth

CG Model Details

The coarse-grained (CG) models used in this study were systematically parameterized from reference all-atom simulations. We first describe the atomistic simulations used, then the procedure to train and simulate the coarse-grained models.

All-atom simulation details

All-atom simulations of a single I-BAR domain of IRSp53 interacting with a fully solvated, periodic lipid bilayer were run using GROMACS (version 5.0) (1). Initially, a lipid bilayer composed of 75% 1,2-dioleoyl-sn-glycero-3-phosphocholine (DOPC), 20% 1,2-dioleoyl-sn-glycero-3-phosphoserine (DOPS), and 5% Phosphatidylinositol-4,5-diphosphate ($PI(4,5)P_2$) was generated using the CHARMM-GUI and equilibrated using the CHARMM-GUI scheme of sequentially restrained simulations (2-6). Next, the I-BAR domain of IRSp53 (PDB: 2YKT(7)) was added to the membrane, and solvated with 150 mM NaCl using GROMACS tools (1). Production simulations were run at 298 K at 1 atm using a Nose-Hoover thermostat and the Parrinello-Rahman barostat implemented with corresponding 1 ps and 5.0 ps coupling constants in GROMACS (1, 8, 9). The CHARMM36 force-field was used in all simulations as well (10-12).

CG model details

A coarse-grained map of I-BAR domain of IRSp53 was created using Essential Dynamics Coarse-graining (ED-CG) using 24 beads per monomer (13). This number of beads was chosen to reproduced to maintain a similar resolution between the protein and lipid model, which has been thoroughly described ref (14). The ED-CG protocol generates a mapping dividing the protein along its primary sequence by minimizing the residual (shown in Eq. 1) describing the fluctuations between beads.

$$\chi^2 = \frac{1}{3N}\sum_{I=1}^{N}\frac{1}{n_t}\sum_{t=1}^{n_t}\left(\sum_{i\in I}\sum_{j\geq i\in I}\left|\Delta r_i^{ED}(t) - \Delta r_j^{ED}(t)\right|^2\right) \quad (1)$$

where N is the number of CG sites, n_t is the number of configuration, and Δr_i^{ED} is the displacement from equilibrium of the ith CG site at configuration t. The protocol used here first maps each residue to the carbon-alpha atom of the residue backbone, then maps multiple carbon-alpha atoms to a single bead resulting in approximately 10 residues per bead. For example, the boundaries for the first bead are the first residue and the fourth residue i.e. the first three residues' carbon alphas map to the first bead. As a result of a steepest descent and simulated annealing minimization scheme, the residue boundaries between beads are as follows, 1st, 4th, 8th, 20th 35th, 48th, 63rd, 77th, 90th, 105th, 114th, 127th, 138th, 147th, 152nd, 156th, 160th, 167th, 177th, 190th, 202nd, 216th, 226th, and 236th. The spacing is not regular as ED-CG optimizes these boundaries to maximally capture the atomistic fluctuations in the protein. The intraprotein interactions are parameterized using a hetero-elastic network model parameterized using the all-atom simulations (15). Parameters, k_{ij} and b_{ij} shown in Eq. 2, between each pair of CG protein beads are determined to reproduce the fluctuations

of the CG beads in the mapped all-atom trajectory. In Table 1, the intraprotein elastic network parameters are shown.

$$U_b(r_{ij}) = k_{ij}(r_{ij} - b_{ij})^2 \quad (2)$$

The interprotein and protein-lipid (nonbonded) interactions use a shifted-force 10-6 Lennard Jones potential defined below (16). Both interprotein and protein-lipid interactions used a sigma value of 1.5 nm, which was the most probable distance between mapped protein beads to the mapped lipid head groups. The nonbonded interaction cutoff was assumed to be 2σ. The epsilon values of the protein-lipid interactions were investigated as described in the main document. The interprotein interactions were the repulsive portion of the protein-lipid interaction.

$$U_{NB} = U_{LJ}(r_{ij}) - U_{LJ}(r_C) - (r - r_c)\, F_{LJ}(r_c), \qquad r < r_C \quad (3)$$

$$U_{LJ}(r_{ij}) = 4\epsilon\left[\left(\frac{\sigma}{r_{ij}}\right)^{10} - \left(\frac{\sigma}{r_{ij}}\right)^{6}\right] \quad \text{and} \quad F_{LJ}(r_{ij}) = -U'_{LJ}(r_{ij}) \quad (4)$$

The initial configurations for each system were created by placing lipids on equally spaced points in the desired geometry (e.g., cylinder) and equilibrating under zero membrane tension when applicable. Proteins were subsequently added to the equilibrated lipid bilayer system. CG simulations were run using the LAMMPS MD engine and the Langevin thermostat with temperature dampening parameter of 5000fs and Parrinello-Rahman barostat with pressure dampening parameter of 50,000fs (8, 17, 18). The timescale of the production simulations was at least 30 million steps with a coarse-grained timestep of 5 fs, but varied based on the geometry and the time required to converge order parameters statistics described in the main text.

MesM-P Model Details

The MesM-P model leverages successes of the original MesM-P model with three major changes: no solvent, softer 10-2 Lennard-Jones potential, and shorter discretization length (19). We set the discretization of the membrane mesh to approximately 3 nm, based on the dimensions of the I-BAR domain of IRSp53 (7). Next, we parametrize the I-BAR domain model as a linear chain of MesM-P particles with varied radii. The protein-membrane interactions use a shifted-force 4-2 Lennard Jones potential similar to that shown above. In the protein-membrane interactions, we use values of sigma equal to 2.67, 2.90, and 3.12 nm and corresponding values of epsilon equal to 1.0, 1.25, and 1.5 kcal/mol, which capture the shape and aggregation behavior of the I-BAR domain as shown in the main text. The protein-protein interactions were the repulsive portion of the protein membrane interaction with the same varied sigma values to maintain the shape of the I-BAR domains.

The initial configurations for each system were made by placing membrane beads on a hexagonal lattice in the desired geometry and equilibrating under zero tension using the Langevin thermostat with temperature dampening parameter of 5000fs and Berendsen barostat with pressure dampening parameter of 50000fs. All systems ran for 5 million timesteps to converge order parameter statistics described in main text. The guiding potential used to generate the membrane bulge as described in the main text was a 325 nm spherical guiding potential slowly moved toward the membrane under zero tension. The spherical surface had a potential form of a 9-3 Lennard Jones similar to the potential shown in Equation 4 with a value of 1 kcal/mol.

CG Protein-Protein Interactions

Thus far, we have assumed that the protein-protein interactions are purely repulsive, i.e., direct attraction between protein beads is not included. In reality, there would be some degree of protein-protein interaction. I-BAR domains are significantly charged proteins, which directly affects the membrane binding behavior. If each CG bead is assigned the mapped net charge, i.e., a simple charge mapping, we find a positively charge protein surface near the membrane and a positive high charge density near the ends of the I-BAR domains, as shown in Fig. S1A. The protein shown similarly to Figure 1A of the main text, and the membrane would lie directly below the I-BAR domain in this view. We note a positively charge protein surface near the membrane and the high charge density near the ends of the I-BAR domain. Additionally, there is a net +3 charge on a CG single bead, which in an atomistic resolution would be delocalized over several residues. In the absence of explicit solvent, we model screened electrostatic interactions between two I-BAR domains with a Yukawa potential with the unknown screening length, κ, shown in Equation 5.

$$V_{Yukawa}(r) = -\frac{q_1 q_2}{4\pi\epsilon_0}\frac{e^{-\kappa r}}{r} \quad (5)$$

In the bulk, we could approximate the experimental screening length corresponding to 20 mM Tris pH 7.5, 60 mM NaCl and 100 mM sucrose buffer, but published studies(20, 21) have shown the effective ion concentration near the membrane is higher than in the bulk. We ran simulations using the possible screening lengths from near bulk ion concentration (κ = 0.15 Å^{-1}) to ~10x increase in effective ion concentration (κ = 0.45 Å^{-1}). We characterize these aggregates using the same order parameter analysis described in the main text and shown in panel B of Fig S1.

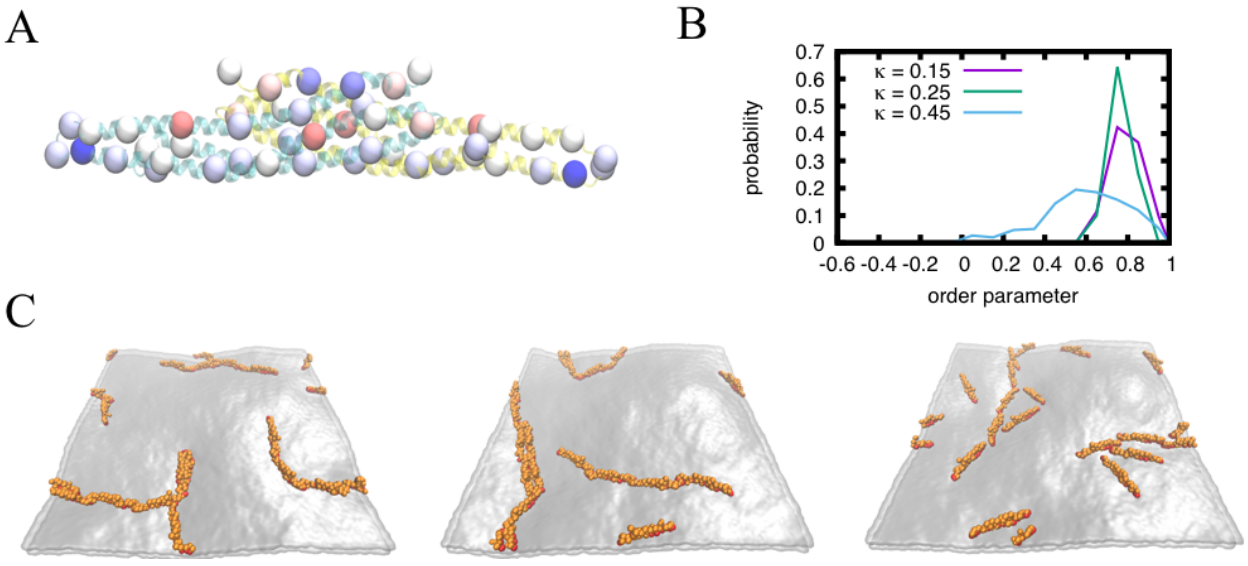

Figure S1. Charge distribution on CG model and snapshots of flat sheet configurations with screened electrostatic interactions. A) Side view of an overlay of the secondary structure of each monomer (cyan and yellow) and CG I-BAR domain colored by charge (+3 charge [blue], -2 [red]) B) probability distribution of inter-protein order parameter for varied screening lengths. C) snapshot of 10% coverage of a 100nm by 100nm flat at varied screening length: 0.15 Å^{-1}, 0.25 Å^{-1}, and 0.45 Å^{-1} from left to right.

As seen in panels B and C of Fig. S1, at low effective ion concentration (κ = 0.15 Å^{-1}), the I-BAR domains begin to form bundled linear aggregates. This behavior is due to an overestimation of the protein-protein interactions because of the low effective salt concentration and the localization of charge on a single CG bead. At 3x bulk ion concentration (κ = 0.25 Å^{-1}), I-BAR domains again form more unbundled linear aggregates with some additional side-to-side character, as additional I-BAR domains move to align opposite charges on the I-BAR domains. This behavior is expected at more reasonable bulk ion concentration. Finally, at 10x bulk ion concentration (κ = 0.45 Å^{-1}), we find mostly linear aggregates again. Thus, when we model the electrostatic interactions between I-BAR domains in this way, we find that aggregation behavior qualitatively agrees with that from purely repulsive excluded volume protein interactions, which is to say that linear tip-to-tip aggregation is dominant and that this behavior is the result of an indirect membrane-mediated force.

Table 1: Heterogenous Elastic Network Model of CG I-BAR Domain. Indices 1-24 and 25-48 are each monomers of the I-BAR dimer.

Bond index	I-BAR site i	I-BAR site j	k_{ij} (kcal/mol/nm)	b_i (nm)
1	1	2	0.157	0.72067
2	1	3	0.051	1.67476
3	1	4	0.035	3.46783
4	1	5	0.025	5.47033
5	1	9	0.022	5.92131
6	1	10	0.026	4.38529
7	1	11	0.037	2.76665
8	1	12	0.932	1.26606
9	1	13	0.038	1.19113
10	1	14	0.006	1.59165
11	1	15	0.004	2.19398
12	1	16	0.006	1.72454
13	1	17	0.008	1.6926
14	1	18	0.726	1.23483
15	1	19	0.849	1.95313
16	1	20	0.042	3.59278
17	1	21	0.031	5.52169
18	1	30	0.024	5.07338
19	1	31	0.034	3.65461
20	1	32	0.026	5.154
21	1	47	0.01	4.80283
22	1	48	0.02	3.94519
23	2	3	5.544	1.28621
24	2	4	0.14	3.19579
25	2	5	0.151	5.18833
26	2	9	0.103	5.62437
27	2	10	0.187	4.18755
28	2	11	1.383	2.70757
29	2	12	1.53	1.46187
30	2	13	0.026	1.73096
31	2	14	0.007	2.0144
32	2	15	0.006	2.49756
33	2	16	0.007	1.80779
34	2	17	0.008	1.81401
35	2	18	0.112	1.25627

36	2	19	7.879	1.64888
37	2	20	0.278	3.23694
38	2	21	0.17	5.14485
39	2	30	0.078	4.68839
40	2	31	0.109	3.16253
41	2	32	0.071	4.68385
42	2	46	0.082	5.60502
43	2	47	0.034	4.34826
44	2	48	0.014	3.53817
45	3	4	0.904	1.96242
46	3	5	0.805	3.93522
47	3	9	0.332	4.34665
48	3	10	0.447	2.93438
49	3	11	22.021	1.63069
50	3	12	11.871	1.33705
51	3	13	0.623	2.63767
52	3	14	0.027	3.17265
53	3	15	0.008	3.66688
54	3	16	0.012	3.04643
55	3	17	0.042	2.9471
56	3	18	7.804	2.01619
57	3	19	45.888	0.93958
58	3	20	30.126	1.9864
59	3	21	0.566	3.89337
60	3	22	4.026	5.69693
61	3	29	10.535	5.58022
62	3	30	0.182	3.47394
63	3	31	0.142	2.002
64	3	32	0.133	3.49711
65	3	33	0.312	5.37109
66	3	45	0.518	5.86174
67	3	46	0.138	4.41816
68	3	47	0.049	3.20181
69	3	48	0.215	2.55673
70	4	5	105.148	2.01061
71	4	6	15.51	4.16504
72	4	7	1.539	5.93097
73	4	8	0.333	4.57014
74	4	9	1.063	2.63051
75	4	10	0.765	1.30486
76	4	11	30.53	1.37257
77	4	12	3.678	2.77714
78	4	13	0.084	4.3937
79	4	14	0.017	4.97111
80	4	15	0.004	5.41424
81	4	16	0.008	4.92109
82	4	17	0.051	4.88414
83	4	18	0.277	3.89841
84	4	19	0.396	2.37234
85	4	20	27.842	1.21186
86	4	21	9.762	2.45227
87	4	22	10.827	4.16281
88	4	23	0.466	5.38916
89	4	28	0.619	5.66204
90	4	29	3.837	3.68981
91	4	30	0.353	1.73921

92	4	31	24.824	1.39215
93	4	32	0.664	2.15746
94	4	33	0.747	3.67121
95	4	34	0.29	5.08677
96	4	44	0.552	5.9
97	4	45	0.802	4.19729
98	4	46	0.472	3.13055
99	4	47	0.202	2.41756
100	4	48	0.005	2.54493
101	5	6	45.734	2.16872
102	5	7	19.259	3.97299
103	5	8	0.304	2.71107
104	5	9	56.299	1.15941
105	5	10	0.313	1.49844
106	5	11	0.191	3.03832
107	5	12	0.251	4.68577
108	5	18	0.674	5.82389
109	5	19	0.567	4.18314
110	5	20	1.119	2.38847
111	5	21	14.294	1.63264
112	5	22	14.076	2.64924
113	5	23	1.869	3.65635
114	5	24	0.724	4.8976
115	5	27	11.57	5.5464
116	5	28	2.268	3.68196
117	5	29	28.581	1.77545
118	5	30	75.667	1.02725
119	5	31	5.607	2.54644
120	5	32	3.063	1.77781
121	5	33	17.757	2.07866
122	5	34	0.802	3.25687
123	5	35	0.371	4.77998
124	5	43	13.979	5.84257
125	5	44	5.312	3.99099
126	5	45	0.675	2.51109
127	5	46	3.462	2.2726
128	5	47	6.301	2.6014
129	5	48	0.004	3.47228
130	6	7	42.079	1.84228
131	6	8	30.511	1.01613
132	6	9	3.442	1.94137
133	6	10	0.913	3.40658
134	6	11	5.248	5.09948
135	6	20	1.263	4.29271
136	6	21	7.913	2.6483
137	6	22	9.276	1.8981
138	6	23	8.22	2.08001
139	6	24	0.509	2.97419
140	6	25	0.001	4.24468
141	6	26	0.007	3.96905
142	6	27	0.157	3.42931
143	6	28	0.305	1.72271
144	6	29	69.728	1.04588
145	6	30	2.679	2.78135
146	6	31	0.5	4.42078
147	6	32	0.268	3.11349

148	6	33	17.334	1.76375
149	6	34	0.655	1.83121
150	6	35	0.233	2.9947
151	6	36	0.168	4.41572
152	6	37	0.117	5.81217
153	6	42	0.242	5.42998
154	6	43	0.224	3.78628
155	6	44	3.3	2.04681
156	6	45	0.555	1.52521
157	6	46	0.296	2.793
158	6	47	0.193	3.90065
159	6	48	0.006	5.04118
160	7	8	0.451	1.50666
161	7	9	12.091	3.51955
162	7	10	0.606	5.13554
163	7	20	0.349	5.89988
164	7	21	0.302	4.04572
165	7	22	0.163	2.50095
166	7	23	3.966	1.55201
167	7	24	0.067	1.45564
168	7	25	0.001	2.55337
169	7	26	0.006	2.20505
170	7	27	0.195	1.91515
171	7	28	22.335	1.40273
172	7	29	0.876	2.59073
173	7	30	0.476	4.44408
174	7	31	0.536	5.98571
175	7	32	0.665	4.54154
176	7	33	0.186	2.89333
177	7	34	1.065	2.11225
178	7	35	2.849	2.26068
179	7	36	0.095	3.11897
180	7	37	0.08	4.35802
181	7	38	0.121	5.2875
182	7	40	0.068	5.66852
183	7	41	0.072	4.96221
184	7	42	0.122	3.805
185	7	43	0.21	2.20225
186	7	44	21.696	1.04014
187	7	45	6.237	2.22118
188	7	46	0.841	3.87393
189	7	47	0.093	5.20378
190	8	9	68.82	2.07031
191	8	10	5.059	3.73619
192	8	11	0.114	5.4378
193	8	20	0.198	4.43006
194	8	21	0.216	2.55541
195	8	22	0.265	1.18895
196	8	23	20.028	1.39495
197	8	24	0.953	2.47085
198	8	25	0.001	3.9512
199	8	26	0.005	3.66932
200	8	27	0.099	3.3883
201	8	28	0.408	2.13006
202	8	29	0.168	1.84705
203	8	30	0.105	3.1741

204	8	31	0.302	4.57779
205	8	32	0.327	3.19577
206	8	33	0.055	2.02378
207	8	34	0.812	2.25619
208	8	35	0.374	3.26643
209	8	36	0.09	4.5016
210	8	37	0.07	5.82844
211	8	42	0.089	5.27441
212	8	43	0.118	3.61619
213	8	44	2.04	1.89881
214	8	45	10.563	1.28128
215	8	46	1.386	2.51662
216	8	47	0.176	3.73432
217	8	48	0.01	4.93198
218	9	10	36.195	1.6856
219	9	11	0.109	3.37636
220	9	12	0.096	5.01007
221	9	19	0.248	4.35228
222	9	20	0.315	2.46801
223	9	21	0.748	0.96599
224	9	22	8.537	1.84659
225	9	23	0.573	3.13593
226	9	24	1.806	4.45707
227	9	25	0.068	5.93647
228	9	26	0.364	5.69178
229	9	27	0.22	5.30425
230	9	28	0.256	3.65102
231	9	29	14.42	2.08446
232	9	30	12.938	1.74039
233	9	31	0.764	2.8325
234	9	32	1.185	1.8969
235	9	33	12.465	2.23946
236	9	34	0.408	3.41697
237	9	35	0.249	4.84781
238	9	43	0.34	5.5861
239	9	44	3.177	3.74528
240	9	45	0.387	2.19358
241	9	46	6.083	1.79227
242	9	47	0.134	2.20616
243	9	48	0.003	3.18199
244	10	11	0.251	1.72458
245	10	12	0.277	3.41935
246	10	13	1.559	5.12251
247	10	14	0.054	5.86738
248	10	16	0.012	5.91282
249	10	17	0.164	5.70769
250	10	18	0.317	4.61824
251	10	19	0.339	2.98906
252	10	20	10.039	1.41065
253	10	21	3.641	1.7958
254	10	22	8.252	3.44731
255	10	23	0.504	4.77085
256	10	28	0.151	5.04749
257	10	29	0.693	3.24221
258	10	30	22.923	1.8423
259	10	31	0.842	2.10261

260	10	32	0.736	2.22537
261	10	33	6.956	3.42676
262	10	34	0.215	4.72064
263	10	44	0.318	5.30907
264	10	45	0.381	3.70361
265	10	46	0.325	2.78998
266	10	47	0.507	2.22394
267	10	48	0.002	2.4968
268	11	12	69.499	1.73151
269	11	13	0.18	3.4337
270	11	14	0.039	4.2105
271	11	15	0.006	4.79613
272	11	16	0.012	4.36094
273	11	17	0.135	4.13693
274	11	18	0.29	3.07696
275	11	19	7.645	1.71042
276	11	20	10.197	1.57909
277	11	21	0.212	3.22352
278	11	22	0.91	5.02939
279	11	29	0.571	4.80664
280	11	30	0.19	3.01484
281	11	31	0.245	2.24014
282	11	32	0.217	3.2867
283	11	33	0.753	4.88777
284	11	45	4.726	5.28011
285	11	46	0.147	4.07452
286	11	47	0.038	2.98872
287	11	48	0.005	2.48693
288	12	13	0.265	1.72076
289	12	14	0.544	2.58217
290	12	15	0.013	3.27135
291	12	16	0.033	2.83371
292	12	17	2.473	2.4968
293	12	18	3.344	1.51159
294	12	19	14.367	1.26472
295	12	20	0.606	2.77833
296	12	21	0.195	4.68308
297	12	30	0.199	4.4599
298	12	31	0.097	3.15395
299	12	32	0.113	4.56429
300	12	46	0.091	5.3872
301	12	47	0.028	4.07016
302	12	48	0.023	3.14937
303	13	14	9.034	1.12617
304	13	15	1.427	1.96107
305	13	16	1.952	1.71085
306	13	17	7.928	1.25037
307	13	18	15.485	1.19683
308	13	19	6.401	2.56683
309	13	20	1.042	4.37675
310	13	31	0.081	4.59449
311	13	47	0.043	5.55008
312	13	48	0.015	4.49255
313	14	15	1.114	0.87504
314	14	16	0.114	0.95271
315	14	17	0.08	1.23054

316	14	18	8.478	1.90432
317	14	19	0.084	3.32567
318	14	20	0.033	5.0789
319	14	31	0.016	5.11535
320	14	48	0.008	5.25932
321	15	16	1.418	1.01069
322	15	17	0.024	1.80918
323	15	18	2.682	2.61775
324	15	19	0.014	3.94812
325	15	20	0.006	5.61121
326	15	31	0.005	5.53346
327	15	48	0.004	5.83937
328	16	17	0.092	1.11345
329	16	18	1.396	1.9107
330	16	19	0.011	3.25537
331	16	20	0.007	4.96865
332	16	31	0.006	4.84759
333	16	48	0.003	5.09493
334	17	18	52.358	1.18257
335	17	19	4.726	2.83744
336	17	20	0.148	4.71213
337	17	31	0.056	4.74436
338	17	47	0.037	5.68279
339	17	48	0.009	4.62069
340	18	19	70.074	1.71897
341	18	20	0.962	3.63203
342	18	21	0.364	5.53978
343	18	30	0.213	5.41822
344	18	31	0.207	3.79104
345	18	32	0.162	5.3013
346	18	47	0.034	4.63895
347	18	48	0.008	3.55428
348	19	20	1.053	1.92276
349	19	21	0.446	3.83058
350	19	22	11.778	5.64721
351	19	29	3.495	5.86731
352	19	30	0.299	3.80701
353	19	31	0.341	2.22356
354	19	32	0.191	3.67124
355	19	33	0.377	5.63841
356	19	45	1.294	5.98858
357	19	46	0.155	4.4064
358	19	47	0.038	2.9988
359	19	48	0.007	2.04434
360	20	21	1.457	1.94337
361	20	22	33.379	3.77768
362	20	23	0.52	5.18225
363	20	28	0.443	5.91179
364	20	29	0.795	4.0181
365	20	30	0.694	2.0643
366	20	31	50.611	1.00424
367	20	32	4.91	1.92312
368	20	33	0.544	3.801
369	20	34	0.353	5.36338
370	20	44	0.481	5.9445
371	20	45	1.584	4.09697

372	20	46	0.536	2.62321
373	20	47	0.066	1.43876
374	20	48	0.003	1.39405
375	21	22	69.497	1.84558
376	21	23	18.368	3.29543
377	21	24	0.098	4.73905
378	21	27	0.262	5.87363
379	21	28	0.571	4.27775
380	21	29	0.346	2.6407
381	21	30	0.665	1.6226
382	21	31	2.838	2.18921
383	21	32	37.178	1.26901
384	21	33	0.173	2.36246
385	21	34	0.482	3.83822
386	21	35	0.545	5.35045
387	21	44	0.62	4.15002
388	21	45	27.453	2.32561
389	21	46	37.503	1.09329
390	21	47	0.114	1.28433
391	21	48	0.005	2.46054
392	22	23	22.771	1.54625
393	22	24	0.327	2.98984
394	22	25	0.001	4.81836
395	22	26	0.005	4.53855
396	22	27	0.115	4.35544
397	22	28	0.397	3.13494
398	22	29	7.824	2.31194
399	22	30	0.79	2.79418
400	22	31	0.846	3.84795
401	22	32	3.316	2.46218
402	22	33	0.417	1.92348
403	22	34	0.477	2.85748
404	22	35	0.149	4.0897
405	22	36	0.094	5.38569
406	22	43	0.123	4.40107
407	22	44	0.346	2.6344
408	22	45	40.304	1.13455
409	22	46	14.711	1.51197
410	22	47	0.296	2.80438
411	22	48	0.216	4.08026
412	23	24	0.049	1.50858
413	23	25	0.001	3.60707
414	23	26	0.005	3.27573
415	23	27	0.168	3.10142
416	23	28	1.339	2.32029
417	23	29	11.199	2.49636
418	23	30	0.472	3.79278
419	23	31	0.189	5.10669
420	23	32	0.228	3.59536
421	23	33	0.362	2.1373
422	23	34	0.454	2.12042
423	23	35	0.067	2.90401
424	23	36	0.063	4.02381
425	23	37	0.051	5.35106
426	23	41	0.04	5.80316
427	23	42	0.062	4.62131

428	23	43	0.096	2.96284
429	23	44	0.212	1.35572
430	23	45	0.38	1.24906
431	23	46	1.708	2.76403
432	23	47	0.086	4.23579
433	23	48	0.027	5.55257
434	24	25	0.001	2.41384
435	24	26	0.002	2.01988
436	24	27	0.023	2.01261
437	24	28	0.087	2.27372
438	24	29	0.133	3.44004
439	24	30	0.118	5.11667
440	24	32	0.044	5.02159
441	24	33	0.05	3.31154
442	24	34	0.708	2.49359
443	24	35	0.024	2.31336
444	24	36	0.024	2.85403
445	24	37	0.019	4.02244
446	24	38	0.02	4.90776
447	24	39	0.015	5.65355
448	24	40	0.016	5.21839
449	24	41	0.017	4.3638
450	24	42	0.017	3.20507
451	24	43	0.012	1.64859
452	24	44	0.019	1.19247
453	24	45	0.035	2.60586
454	24	46	0.098	4.24311
455	24	47	0.026	5.71427
456	25	26	0.023	0.82883
457	25	27	0.487	1.66351
458	25	28	0.002	3.14735
459	25	29	0.002	4.90243
460	25	33	0.001	5.20058
461	25	34	0.002	4.02206
462	25	35	0.011	3.08506
463	25	36	0.013	2.41577
464	25	37	0.002	2.75094
465	25	38	0.001	3.52485
466	25	39	0.001	4.19656
467	25	40	0.001	3.62482
468	25	41	0.001	3.02912
469	25	42	0.002	2.18536
470	25	43	0.199	1.81331
471	25	44	0.002	2.8749
472	25	45	0.001	4.57164
473	26	27	1.664	1.16362
474	26	28	0.01	2.81353
475	26	29	0.008	4.61297
476	26	33	0.007	4.88748
477	26	34	0.009	3.67927
478	26	35	0.025	2.71004
479	26	36	0.309	2.11156
480	26	37	0.01	2.66323
481	26	38	0.008	3.51169
482	26	39	0.006	4.2164
483	26	40	0.006	3.66067

484	26	41	0.009	2.98739
485	26	42	0.02	2.00105
486	26	43	0.564	1.3039
487	26	44	0.006	2.48195
488	26	45	0.005	4.2549
489	26	46	0.021	5.9397
490	27	28	0.971	1.95652
491	27	29	1.24	3.91516
492	27	33	0.405	4.29863
493	27	34	11.562	2.86869
494	27	35	12.199	1.68926
495	27	36	12.468	1.37094
496	27	37	5.177	2.46513
497	27	38	2.35	3.39551
498	27	39	0.688	4.21386
499	27	40	0.738	3.85144
500	27	41	3.186	3.21035
501	27	42	10.64	2.08496
502	27	43	41.98	0.917
503	27	44	35.011	1.94764
504	27	45	0.529	3.84402
505	27	46	1.033	5.64131
506	28	29	102.142	2.00602
507	28	30	26.96	4.1551
508	28	31	1.15	5.90133
509	28	32	2.84	4.50849
510	28	33	1.98	2.60714
511	28	34	23.869	1.24932
512	28	35	8.447	1.3753
513	28	36	0.432	2.74411
514	28	37	0.229	4.17757
515	28	38	0.097	5.08376
516	28	39	0.049	5.93774
517	28	40	0.155	5.70091
518	28	41	0.318	5.07467
519	28	42	0.527	3.91359
520	28	43	2.63	2.36973
521	28	44	59.47	1.21298
522	28	45	18.086	2.41257
523	28	46	1.489	4.16748
524	28	47	0.141	5.47126
525	29	30	48.671	2.16797
526	29	31	34.718	3.95677
527	29	32	11.188	2.67107
528	29	33	0.996	1.14339
529	29	34	0.232	1.50795
530	29	35	0.166	3.0102
531	29	36	0.203	4.64989
532	29	42	0.796	5.81704
533	29	43	1.773	4.1717
534	29	44	19.958	2.38201
535	29	45	20.939	1.55098
536	29	46	6.008	2.68271
537	29	47	3.588	3.77384
538	29	48	0.008	4.92769
539	30	31	85.543	1.82484

540	30	32	63.726	0.99779
541	30	33	12.025	1.94261
542	30	34	6.674	3.43993
543	30	35	3.389	5.06669
544	30	44	0.807	4.26651
545	30	45	1.26	2.55704
546	30	46	25.661	1.90322
547	30	47	9.947	2.17974
548	30	48	0.018	3.14438
549	31	32	1.018	1.53642
550	31	33	4.011	3.52897
551	31	34	0.624	5.1627
552	31	44	0.329	5.85704
553	31	45	0.442	3.96656
554	31	46	0.272	2.47624
555	31	47	2.901	1.54966
556	31	48	0.403	1.87535
557	32	33	61.001	2.06571
558	32	34	16.025	3.74049
559	32	35	13.839	5.36457
560	32	44	0.607	4.35289
561	32	45	1.606	2.44643
562	32	46	0.544	1.15229
563	32	47	11.484	1.44203
564	32	48	0.125	2.64685
565	33	34	0.625	1.6918
566	33	35	0.348	3.31317
567	33	36	0.255	4.96018
568	33	43	0.371	4.32106
569	33	44	0.471	2.45144
570	33	45	10.731	0.97636
571	33	46	3.958	1.96215
572	33	47	4.278	3.26989
573	33	48	0.405	4.55638
574	34	35	0.79	1.64685
575	34	36	0.443	3.34686
576	34	37	0.51	4.88467
577	34	38	0.403	5.76317
578	34	41	0.21	5.72765
579	34	42	0.488	4.53735
580	34	43	7.23	2.93556
581	34	44	14.643	1.38172
582	34	45	8.555	1.81806
583	34	46	1.011	3.52568
584	34	47	0.514	4.89162
585	35	36	48.533	1.74049
586	35	37	1.778	3.28327
587	35	38	0.174	4.14304
588	35	39	0.026	4.99755
589	35	40	0.048	4.8754
590	35	41	0.253	4.21123
591	35	42	0.255	3.06996
592	35	43	2.661	1.73749
593	35	44	6.793	1.58676
594	35	45	0.349	3.20926
595	35	46	1.05	5.0327

596	36	37	82.511	1.55138
597	36	38	0.311	2.42869
598	36	39	0.041	3.28898
599	36	40	0.066	3.1487
600	36	41	0.402	2.53341
601	36	42	6.272	1.50949
602	36	43	3.088	1.29266
603	36	44	1.59	2.77502
604	36	45	0.285	4.68144
605	37	38	8.365	0.94399
606	37	39	1.073	1.82176
607	37	40	0.531	1.65835
608	37	41	3.969	1.29772
609	37	42	3.256	1.12448
610	37	43	0.43	2.41174
611	37	44	0.431	4.19524
612	38	39	0.104	0.95919
613	38	40	0.436	1.09773
614	38	41	1.498	1.26418
615	38	42	2.226	1.82715
616	38	43	1.065	3.3145
617	38	44	0.851	5.11477
618	39	40	4.197	0.89083
619	39	41	1.564	1.59492
620	39	42	0.629	2.5102
621	39	43	0.433	4.10042
622	39	44	0.273	5.93457
623	40	41	3.825	1.0315
624	40	42	2.769	2.08683
625	40	43	0.242	3.73676
626	40	44	0.313	5.61278
627	41	42	14.881	1.22155
628	41	43	0.985	2.92954
629	41	44	0.28	4.83764
630	42	43	70.754	1.71484
631	42	44	0.619	3.62667
632	42	45	0.206	5.54581
633	43	44	0.841	1.91735
634	43	45	0.305	3.8395
635	43	46	0.495	5.63309
636	44	45	1.009	1.94795
637	44	46	13.447	3.77456
638	44	47	0.107	5.22822
639	45	46	33.545	1.84665
640	45	47	0.414	3.3115
641	45	48	0.106	4.642
642	46	47	0.382	1.53726
643	46	48	0.117	2.9303
644	47	48	0.036	1.48032

Supplemental References

1. Abraham, M. J., T. Murtola, R. Schulz, S. Páll, J. C. Smith, B. Hess, and E. Lindahl. 2015. GROMACS: High performance molecular simulations through multi-level parallelism from laptops to supercomputers. *SoftwareX.* 1-2:19-25.
2. Jo, S., T. Kim, and W. Im. 2007. Automated builder and database of protein/membrane complexes for molecular dynamics simulations. *PLoS One.* 2:e880.
3. Jo, S., T. Kim, V. G. Iyer, and W. Im. 2008. CHARMM-GUI: a web-based graphical user interface for CHARMM. *J Comput Chem.* 29:1859-1865.
4. Jo, S., J. B. Lim, J. B. Klauda, and W. Im. 2009. CHARMM-GUI Membrane Builder for mixed bilayers and its application to yeast membranes. *Biophys J.* 97:50-58.
5. Lee, J., X. Cheng, J. M. Swails, M. S. Yeom, P. K. Eastman, J. A. Lemkul, S. Wei, J. Buckner, J. C. Jeong, Y. Qi, S. Jo, V. S. Pande, D. A. Case, C. L. Brooks, 3rd, A. D. MacKerell, Jr., J. B. Klauda, and W. Im. 2016. CHARMM-GUI Input Generator for NAMD, GROMACS, AMBER, OpenMM, and CHARMM/OpenMM Simulations Using the CHARMM36 Additive Force Field. *J Chem Theory Comput.* 12:405-413.
6. Wu, E. L., X. Cheng, S. Jo, H. Rui, K. C. Song, E. M. Davila-Contreras, Y. Qi, J. Lee, V. Monje-Galvan, R. M. Venable, J. B. Klauda, and W. Im. 2014. CHARMM-GUI Membrane Builder toward realistic biological membrane simulations. *J Comput Chem.* 35:1997-2004.
7. de Groot, J. C., K. Schluter, Y. Carius, C. Quedenau, D. Vingadassalom, J. Faix, S. M. Weiss, J. Reichelt, C. Standfuss-Gabisch, C. F. Lesser, J. M. Leong, D. W. Heinz, K. Bussow, and T. E. Stradal. 2011. Structural basis for complex formation between human IRSp53 and the translocated intimin receptor Tir of enterohemorrhagic E. coli. *Structure.* 19:1294-1306.
8. Parrinello, M., and A. Rahman. 1981. Polymorphic Transitions in Single-Crystals - a New Molecular-Dynamics Method. *Journal of Applied Physics.* 52:7182-7190.
9. Smit, B., and D. Frenkel. 2001. Understanding Molecular Simulation: From Algorithms to Applications. Elsevier.
10. Best, R. B., X. Zhu, J. Shim, P. E. Lopes, J. Mittal, M. Feig, and A. D. Mackerell, Jr. 2012. Optimization of the additive CHARMM all-atom protein force field targeting improved sampling of the backbone phi, psi and side-chain chi(1) and chi(2) dihedral angles. *J Chem Theory Comput.* 8:3257-3273.
11. Klauda, J. B., R. M. Venable, J. A. Freites, J. W. O'Connor, D. J. Tobias, C. Mondragon-Ramirez, I. Vorobyov, A. D. MacKerell, Jr., and R. W. Pastor. 2010. Update of the CHARMM all-atom additive force field for lipids: validation on six lipid types. *J Phys Chem B.* 114:7830-7843.
12. MacKerell, A. D., D. Bashford, M. Bellott, R. L. Dunbrack, J. D. Evanseck, M. J. Field, S. Fischer, J. Gao, H. Guo, S. Ha, D. Joseph-McCarthy, L. Kuchnir, K. Kuczera, F. T. Lau, C. Mattos, S. Michnick, T. Ngo, D. T. Nguyen, B. Prodhom, W. E. Reiher, B. Roux, M. Schlenkrich, J. C. Smith, R. Stote, J. Straub, M. Watanabe, J. Wiorkiewicz-Kuczera, D. Yin, and M. Karplus. 1998. All-atom empirical potential for molecular modeling and dynamics studies of proteins. *J Phys Chem B.* 102:3586-3616.
13. Zhang, Z., L. Lu, W. G. Noid, V. Krishna, J. Pfaendtner, and G. A. Voth. 2008. A systematic methodology for defining coarse-grained sites in large biomolecules. *Biophys J.* 95:5073-5083.

14. Srivastava, A., and G. A. Voth. 2013. A Hybrid Approach for Highly Coarse-grained Lipid Bilayer Models. *J Chem Theory Comput.* 9:750-765.
15. Lyman, E., J. Pfaendtner, and G. A. Voth. 2008. Systematic multiscale parameterization of heterogeneous elastic network models of proteins. *Biophys J.* 95:4183-4192.
16. Allen, M. P., and D. J. Tildesley. 1989. Computer simulation of liquids. Clarendon Press, Oxford.
17. Plimpton, S. 1995. Fast Parallel Algorithms for Short-Range Molecular Dynamics. *Journal of Computational Physics.* 117:1-19.
18. Dunweg, B., and W. Paul. 1991. Brownian Dynamics Simulations without Gaussian Random Numbers. *International Journal of Modern Physics C.* 2:817-827.
19. Davtyan, A., M. Simunovic, and G. A. Voth. 2017. The mesoscopic membrane with proteins (MesM-P) model. *The Journal of Chemical Physics.* 147:044101.
20. Böckmann, R. A., A. Hac, T. Heimburg, and H. Grubmüller. 2003. Effect of Sodium Chloride on a Lipid Bilayer. *Biophysical Journal.* 85:1647-1655.
21. Pandit, S. A., D. Bostick, and M. L. Berkowitz. 2003. Mixed Bilayer Containing Dipalmitoylphosphatidylcholine and Dipalmitoylphosphatidylserine: Lipid Complexation, Ion Binding, and Electrostatics. *Biophysical Journal.* 85:3120-3131.